Bachelor Thesis

Numerical simulation of directed quantum tunnelling

Melvin Hodžić

written at the Department of Physics
Karl Franzens University of Graz

under the supervision of
Ao.Univ.-Prof. Mag. Dr. Ulrich Hohenester

Graz, May 2021

Abstract

Quantum tunnelling is a quantum mechanical effect where a wave function propagates through a potential barrier. Therefore, the probability to find a particle outside a potential well is non-zero, despite the energy of the particle being insufficient to overcome the barrier classically. This phenomenon is generally regarded as a process that occurs without loss in energy, which is in contrast to the findings made by the realization and study of the world's smallest molecular motor. For this construct rotations with a high degree of directionality were observed, even when crossing the limits from the classical to the quantum tunnelling regime.

In this bachelor thesis the idea of directed quantum tunnelling in a periodic, asymmetric potential is investigated by simulating the motion of a single particle inside this specified potential. This is achieved via a Matlab implementation of the Crank-Nicoloson scheme for the numerical solution of the time dependant Schrödinger equation. The ground and first excited state of a single, triangular potential well are used as initial wave functions. Thereby, only when using the latter, a preferred direction of the tunnel motion is observed. This indicates that the transition from the ground to the first excited state is connected to a gain of directionality. To quantify the result obtained from this two-level system, the tunnel rates for a reduced potential of three wells are calculated. In doing so, no asymmetry regarding the rates has been obtained. This implies that subsequent studies on energy dissipation during tunnelling events require an expansion to a more-level system or the inclusion of environment couplings.

Contents

Chapter 1

Introduction

The realization and investigation of the world's smallest molecular motor, consisting of just 16 atoms, lead to insights regarding directed motion, not only with respect to the classical but also the quantum tunnelling regime. Consisting of a single acetylene (C_2H_2) rotor and a chiral PdGa(111) stator, the motor's behaviour is tracked by scanning tunnelling microscopy (STM). With this setup a high degree of directionality, over 97%, for the observed rotations is reported in [1] even below the limits of 17 K and 30 mV bias voltage, which indicate the cross-over from classical motion to quantum tunnelling. This is insofar remarkable, as quantum mechanical tunnelling usually occurs without any loss of energy, which would be verified by no preferred direction of rotation. However, as the rotations occur almost purely in the same direction, the motor enables the study of energy dissipation in quantum tunnelling processes, which motivates the topic of this thesis.

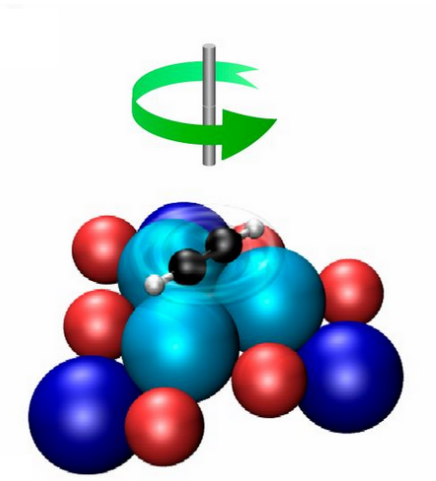

Fig. 1.1: Sketch of the acetylene (C_2H_2) rotor on the PdGA(111) stator. Taken from [1]

In this work directed quantum tunnelling inside a periodic, asymmetric potential is elaborated on. In order to simulate the time development and, thereby, tunnel motion in such a potential, the Crank-Nicoloson method [2] is implemented via Matlab [3] with the ground and first excited state of the single well as initial wave functions. To quantify the obtained result and gain further insight about the origin of directed quantum tunnelling, the tunnel rates for a two-level system using a reduced potential of three triangular wells are calculated.

Structurally, this thesis is initiated by a theory chapter, where the necessary quantum mechanics as well as background information to the single, triangular well and the periodic, asymmetric potential with regards to directed motion are given. This is followed up by the derivation and implementation of the numerical method for the solution of the time dependant Schrödinger equation, namely the Crank-Nicoloson scheme. Eventually, the obtained results allowing to discuss directed quantum tunnelling are presented in a series of plots together with the tunnel rate matrix.

Chapter 2

Theory

In this chapter quantum mechanics basics are briefly summarized, in order to discuss the problem of the asymmetric, triangular well. The single well is then expanded to the periodic and asymmetric ratchet potential. Finally, directed motion and quantum tunnelling in such a potential is discussed.

2.1 The 1-dimensional Schrödinger equation

To describe the time development of the state of a quantum mechanical system, the time dependant Schrödinger equation (TDSE) is used. In position space representation and one spatial dimension this partial differential equation has the form

$$\mathrm{i}\hbar\frac{\partial}{\partial t}\psi(x,t) = -\frac{\hbar^2}{2m}\frac{\partial^2}{\partial x^2}\psi(x,t) + V(x,t)\psi(x,t) \tag{2.1}$$

with $\mathrm{i} = \sqrt{-1}$ being the imaginary number, $\hbar$ the reduced Planck constant, m the mass of the particle, $V(x,t)$ the potential and $\psi(x,t)$ the wave function. The square of the absolute value $|\psi(x,t)|^2$ represents the probability density of finding the particle at a time t at position x.
The right-hand side can be written in terms of the Hamilton operator

$$\hat{H}(x,t) = -\frac{\hbar^2}{2m}\frac{\partial^2}{\partial x^2} + V(x,t) = \hat{T} + \hat{V}. \tag{2.2}$$

Here, $\hat{T}$ represents the kinetic energy of the particle and $\hat{V}$ the potential, in which the particle is moving. If $\hat{H}$ is not time dependant, the time development of a general state is described by

$$\psi(x,t) = \hat{U}(t)\psi(x,0) = e^{-\frac{i\hat{H}t}{\hbar}}\psi(x,0). \tag{2.3}$$

In this form it can be seen that the Schrödinger equation provides information about a state $\psi(x,t)$ at a time t ≥ 0, when the initial state at t $= 0$ is known. $\hat{U}(t)$ is called the time evolution operator or propagator and fulfils the condition of unitarity $\hat{\mathrm{U}}^{\dagger}(\mathrm{t})\hat{\mathrm{U}}(\mathrm{t}) = \hat{\mathbb{1}}$. With this property, it is ensured that the norm of the wave function does not change.

$$|\psi(x,t)|^2 = |\psi(x,0)|^2 \tag{2.4}$$

Additionally, for the case that the Hamilton operator is time independent, we can formulate the stationary Schrödinger equation using Dirac notation

$$\hat{H}\,|\varphi_n\rangle = E_n\,|\varphi_n\rangle\,, \tag{2.5}$$

where E_n is the eigenvalue belonging to the eigenstate $|\varphi_n\rangle$. The application of a hermitian operator to a state corresponds to the measurement of a physical observable. In this context, the possible results of a single measurement are the eigenvalues and hereafter the system can be found in the respective eigenstate. Due to the hermiticity of $\hat{H}$, the entity of all eigenstates form a basis of the state space. This means that a solution of the Schrödinger equation can be written as a linear combination of eigenstates:

$$|\psi(t)\rangle = \sum_n c_n(t)\,|\varphi_n\rangle \tag{2.6}$$

with $c_n(t)$ being the development coefficients. It is important to notice that a linear combination of eigenstates to different eigenvalues is not an eigenstate itself. With that, the expectation value of the Hamilton operator can be calculated:

$$E = \langle\psi(t)|\hat{H}|\psi(t)\rangle. \tag{2.7}$$

For $\hat{H}$ the corresponding observable is the energy. Therefore, E_n are the eigenenergies of the system and the expectation value E is equal to the total energy of the system in the state $|\psi(t)\rangle$ [4, pp. 55-58, 62-69].

2.2 The triangular potential well

In quantum mechanics potential well problems are commonly used to describe and discuss the physics of a system. Here, a potential well can assume different shapes such as a box, a parabola or more complex mathematical functions like the Morse potential. The well guides the motion of a particle. This confinement is particularly important when spatial dimensions approach the atomic scale, as the particle's properties change. It is for example important to notice that for finite barriers there is a non-zero probability of finding the particle outside the well, even though

its total energy is less than the potential energy barrier. This behaviour is forbidden in the classical description and is called quantum tunnelling. The tunnelling effect comes to use in various technical applications such as Scanning Tunnelling Microscopy (STM), tunnel diodes and flash memory. Moreover, the effect enjoys increasing popularity in the life sciences as findings in the fields of molecular and biological evolution and prebiotic chemistry show [4, pp. 88-97] [5, pp. 4-5] [6] [7] [8] [9].

In this work the directionality of motion of a particle inside a periodic triangular potential well is discussed. The single well consists of a linearly increasing potential $V(x)$ bound by an infinite barrier at $x = 0$. The potential at $x > 0$ is for example created by a constant electric field:

$$V(x) = q\varepsilon x. \tag{2.8}$$

This well finds use in semi-conductor and transistor design. For instance, in the high-electron-mobility transistor (HEMT) the combination of different semi-conducting materials leads to the confinement of electrons to the triangular well. For such a potential an analytical solution of the Schrödinger equation eq. 2.5 is provided by the Airy functions. These functions are linearly independent solutions to the Airy differential equation:

$$y'' - xy = 0. \tag{2.9}$$

The solution is obtained by assuming a power series form, indices shifting and determining the coefficients via a recurrence relation. Hereafter, the solution can be written as $y = c_1\mathrm{Ai}(x) + c_2\mathrm{Bi}(x)$, with the Airy function of the first kind $A_i(x)$ being

$$\mathrm{Ai}(x) = \frac{1}{3^{2/3}\Gamma\left(\frac{2}{3}\right)}\left(1 + \frac{x^3}{6} + \frac{x^6}{180} + \cdots\right) - \frac{1}{3^{1/3}\Gamma\left(\frac{1}{3}\right)}\left(x + \frac{x^4}{12} + \frac{x^7}{504} + \cdots\right) \tag{2.10}$$

and the Airy function of the second kind $B_i(x)$

$$\mathrm{Bi}(x) = \frac{1}{3^{1/6}\Gamma\left(\frac{2}{3}\right)}\left(1 + \frac{x^3}{6} + \frac{x^6}{180} + \cdots\right) + \frac{3^{1/6}}{\Gamma\left(\frac{1}{3}\right)}\left(x + \frac{x^4}{12} + \frac{x^7}{504} + \cdots\right). \tag{2.11}$$

Here, $\Gamma(x)$ is the gamma function. A plot of the two functions can be seen in fig. 2.1 below.

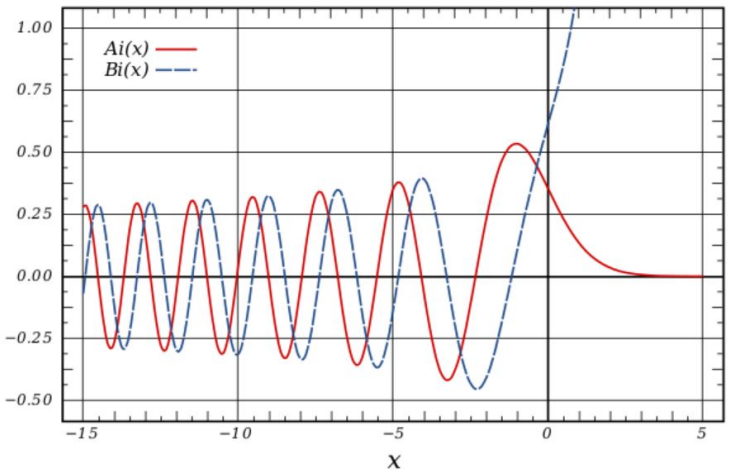

Fig. 2.1: Plot of the Airy functions of the first and second kind. Taken from [10]

Inserting expression eq. 2.8 in eq. 2.5 in position space representation yields

$$-\frac{\hbar^2}{2m}\frac{d^2\psi_n(x)}{dx^2} + q\varepsilon x\psi_n(x) = E_n\psi_n(x). \tag{2.12}$$

This equation can be rearranged to the Airy equation form eq. 2.9, for which the solution is known. Introducing $z = \sqrt[3]{\frac{2mq\varepsilon}{\hbar^2}}\left(x - \frac{E_n}{q\varepsilon}\right)$ allows eq. 2.12 to be written as

$$\frac{d^2\psi_n(z)}{dz^2} = \psi_n(z)z. \tag{2.13}$$

The general solution $\psi_n(z) = A\,\mathrm{Ai}(z) + B\,\mathrm{Bi}(z)$ is given by superposing the Airy functions, where A and B are constants. From looking at the plot in fig. 2.1, it can be seen that the Airy function of the second kind $\mathrm{Bi}(z)$ diverges for positive z values. Therefore, to ensure normalisation $\mathrm{Bi}(z)$ needs to be rejected. This leads to only $\mathrm{Ai}(z)$ being part of the solution, which means in terms of x

$$\psi_n(x) = A\mathrm{Ai}\left[\sqrt[3]{\frac{2mq\varepsilon}{\hbar^2}}\left(x - \frac{E_n}{q\varepsilon}\right)\right]. \tag{2.14}$$

From this an expression for the energy eigenvalues E_n can be derived. Due to the infinite barrier at $x = 0$ $\psi_n(0) = 0$ is valid. As the constant A can not be zero, the condition

$$\mathrm{Ai}\left[-\sqrt[3]{\frac{2mq\varepsilon}{\hbar^2}}\frac{E_n}{q\varepsilon}\right] = 0 \tag{2.15}$$

must be satisfied. With α_n denoting the x-coordinate of the n-th zero of $\mathrm{Ai}(x)$, which can be seen in fig. 2.1, the energy eigenvalues are calculated via

$$E_n = -\alpha_n \sqrt[3]{\frac{\hbar^2 q^2 \varepsilon^2}{2m}}. \tag{2.16}$$

The normalisation constant A can be shown to be $A = \left(\frac{\sqrt[3]{\frac{2mq\varepsilon}{\hbar^2}}}{\mathrm{Ai}'^2\left[-\sqrt[3]{\frac{2mq\varepsilon}{\hbar^2}}\frac{E_n}{q\varepsilon}\right]} \right)^{1/2}$, which gives the eigenfunctions for a particle in a triangular potential with an infinite barrier

$$\psi_n(x) = \left(\frac{\sqrt[3]{\frac{2mq\varepsilon}{\hbar^2}}}{\mathrm{Ai}'^2\left[-\sqrt[3]{\frac{2mq\varepsilon}{\hbar^2}}\frac{E_n}{q\varepsilon}\right]} \right)^{1/2} \mathrm{Ai}\left[\sqrt[3]{\frac{2mq\varepsilon}{\hbar^2}} \left(x - \frac{E_n}{q\varepsilon} \right) \right]. \tag{2.17}$$

The energy level diagram for the triangular potential well can be seen in fig. 2.2 below, where the potential represents the conduction band edge of a semiconductor. [10, pp. 8-15] [11]

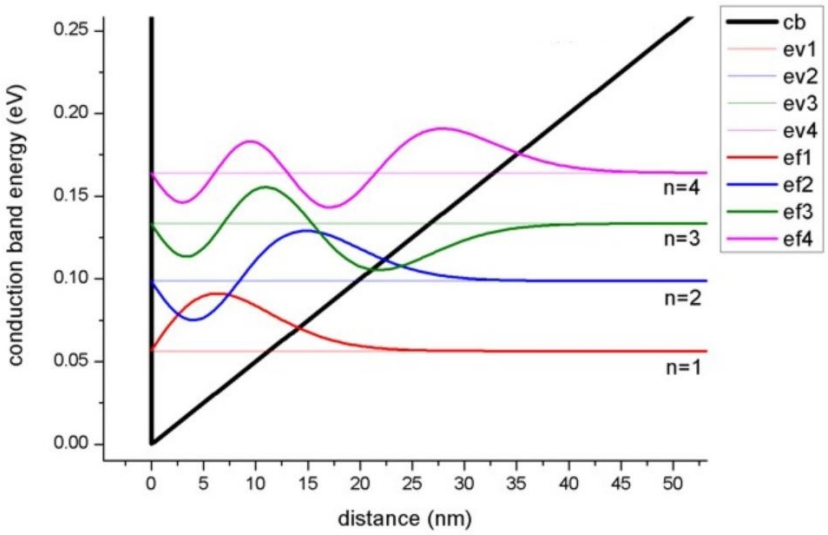

Fig. 2.2: The four lowest energy eigenvalues and the corresponding eigenfunctions of the triangular potential well. An electric field of 5 MV/m and an effective electron mass of $0.067m_0$(GaAs) have been used. Taken from [11]

Moreover, the triangular potential well is taken into consideration when it comes to approximating the Lennard-Jones potential. This potential describes the interaction between particles as a function of distance based on physical arguments, mainly Pauli repulsion and van der Waals attraction. When implementing the Lennard-Jones

potential in a simulation, one is confronted with the problem of correctly handling its long range tail. Due to the triangular potential having no such tail, a much easier and computational cheaper implementation in molecular dynamic simulations is achieved. However, the triangular well potential has been shown to reproduce similar thermodynamic properties of molecular systems as the Lennard-Jones potential, particularly when dealing with noble gases. Additionally, both potentials have in common that they are asymmetric. In fig. 2.3 below both potentials are plotted, which allows to see the similarities in shape [12].

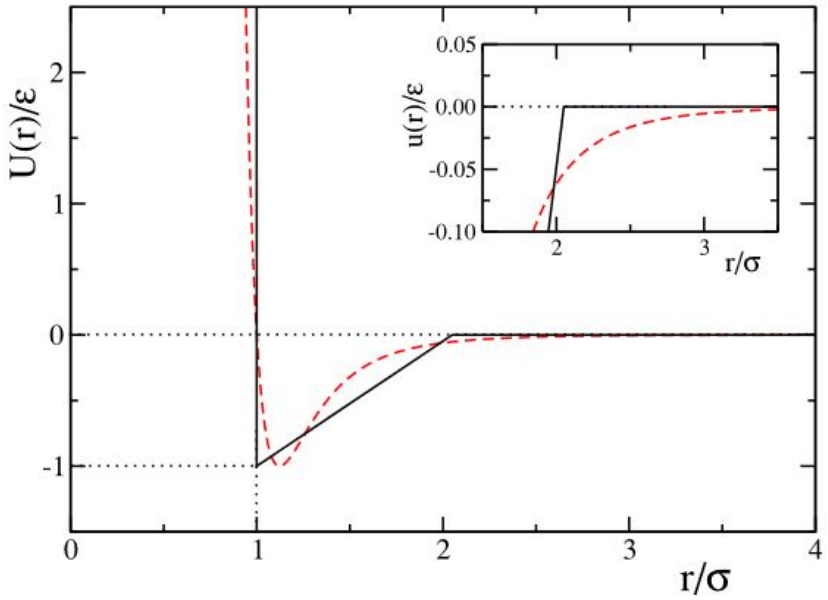

Fig. 2.3: Lennard-Jones potential (red dashed line) compared to the triangular potential (black solid line) as a function of distance r over the particle size parameter σ. Taken from [12]

2.3 Asymmetry and directed motion

The aspect of asymmetry is crucial when discussing directionality of motion. Putting several triangular potential wells together periodically leads to the formation of the ratchet potential. Particles under the influence of this sawtooth shaped potential can produce a finite net flow by converting an undirected energy input into directed motion. Based on classical mechanics, one type of ratchet model is the thermal ratchet. Here, the potential is periodically switched on and off. In the on-potential period the particle is located at one potential bottom, whereas in the off-potential period it

diffuses symmetrically. When the potential is switched on again, the position of the particle is asymmetric and a mean displacement in the direction of the steeper slope of the sawtooth potential appears. A schematic drawing of such a potential can be seen in fig. 2.4 below. Moreover, for low temperatures and micro- or meso-scopic systems quantum mechanical effects come into play. This has lead to the proposal of a quantum mechanical analogue in form of a tight-binding model with an asymmetric periodic potential and periodic on- and off-switching of its amplitude. In the on-potential period the flow oscillates in each valley of the potential. By turning the potential off the flow becomes constant and contributes to the net flow. Without a heat bath the magnitude and direction of the flow are random, which lead to a vanishing net flow. On the other hand, if the system is in contact with a heat bath, it becomes stationary and the flow in every off-potential period is the same. This leads to a finite net flow with temperature dependant direction, even in the limit of $T \to 0$. This behaviour is in clear contrast to the classical thermal ratchet, which is why it can be stated that the occurring quantum mechanical effects result from the interaction with the heat bath [13].

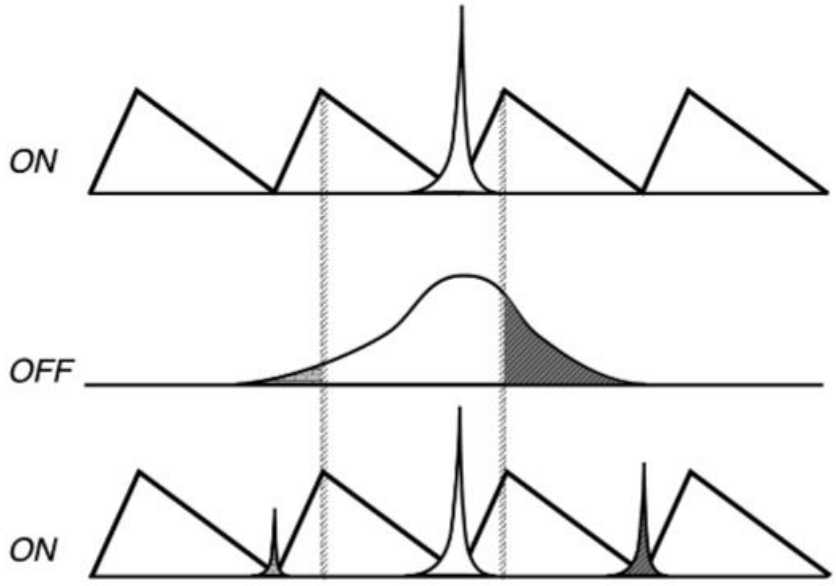

Fig. 2.4: The classical thermal ratchet. Due to the flashing and asymmetry of the potential the distribution of the particle density changes stronger in the direction of the steeper slope (e.g. to the right). Taken from [14, p. 1]

Another classical example is the mechanical ratchet, where correlated noise such as an AC force causes finite net flow. This is the result of asymmetric static frictional

forces due to the steepest slopes of the potential. Therefore, the direction is opposite to that of the thermal ratchet. The quantum mechanical analogue in this case is created by a sawtooth shaped static potential with a weak external AC field. Under the assumption of absolute zero temperature and an adiabatic regime the tunnelling probabilities from one bottom of the periodic potential to the neighbouring ones can be calculated. Doing so, the impact of the AC field is shown by a larger tunnelling probability to the steeper slope direction. Additionally, with heat bath interaction the tunnelling events are independent from each other, which leads to a finite net flow due to asymmetric tunnelling probabilities. Here, the direction is the steeper slope direction, which is opposite to that of the classical mechanical ratchet. [13]

The study of ratchets is of particular interest for the field of molecular motors. These microscopic machines appear in nature in form of motor proteins but are also realized artificially. Recently, a motor consisting of just 16 atoms has been created and investigated via scanning tunnelling microscopy (STM). In order to do so, a single, symmetric acetylene (C_2H_2) rotor is anchored to a chiral stator provided by a PdGa(111) surface. This basically triangular surface is made up of three layers, the first containing 3 Pd atoms, the second six Ga atoms and the third again 3 Pd atoms. Due to this structure, spatial inversion symmetry is broken, which induces the rotation of the acetylene molecule independently of the STM-tip condition and position. The rotation mechanism operates in the classical (CR) as well as tunnelling regime (TR). For the CR the rotations can be powered by thermal or electrical excitations. For a low bias voltage an Arrhenius characteristic of the temperature dependency of the rotation frequency and an exponential increase of the frequency above a voltage of 30 mV. Moreover, for the directionality a rapid drop is observed, when thermally activated rotations start to contribute, which is the case for a temperature above 17 K. The random thermal rotations occur due to the system being in thermal equilibrium, which prohibits unidirectional motion according to the second law of thermodynamics. On the other hand, rotations induced by inelastic electron tunnelling (IET) resulting from the STM-tip only become gradually non-directional for a bias voltage above 30 mV. The rotation events driven by this non-cyclic, directionless and position independent energy input are represented by a static, periodic and asymmetric ratchet potential [1].

With that, the nearly perfect unidirectional rotation of the acetylene rotor in the tunnelling regime is discussed. Below a temperature of 17 K and a bias voltage of 30 mV the rotation frequency remains constant. This means that the rotation events are observed, despite the supplied energy being lower than the energy required to overcome the potential barrier and to set the rotor in motion, which indicates quantum tunnelling. However, tunnel motion usually occurs without energy dissipation,

which is why no preferred rotation should be expected. Nevertheless, for the observed molecular motor, quantum tunnelling rotations with a high directionality of over 97 % in the direction of the steeper slope have been reported. This implies that the directional TR rotation must be a non-equilibrium process with energy dissipation. In this context it is assumed that the energy is used to excite the rotor from the rotational ground state to a bound mode. Therefore, this molecular motor opens up investigations regarding energy dissipation during tunnelling events and quite possibly energy harvesting at the atomic scale [1].

Chapter 3

Numerical methods

In the following the computational method for solving the time-dependant Schrödinger equation, the Crank-Nicoloson method, and the solution of a tridiagonal system of equations via LU-decomposition combined with forward- and back-substitution are explained. This is followed up by a Matlab implementation of the described schemes, which was provided to me by my supervisor Prof. Hohenester and was further modified by extracting parts of the code to Matlab functions. Here, for the numerical calculations Planck's constant $\hbar$ is set to 1.

3.1 Crank-Nicoloson method

Treating a partial differential equation problem numerically requires discretization, which can be achieved by a uniform grid in space and time

$$x_j = j\Delta x \quad \text{with} \quad j = 1, ..., J \tag{3.1}$$

$$t_n = n\Delta t \quad \text{with} \quad n = 1, ..., N \tag{3.2}$$

with x_j being the spatial and t_n being the time grid points. Δx is the step size in space and Δt the step size in time. With that, the wave function values for each grid point j,n are written as

$$\psi_j^n = \psi(x_j, t_n) \tag{3.3}$$

and represented by a column vector for every time step. Moreover, applying numerical methods to the TDSE necessitates the transformation of the Hamilton operator $\hat{H}$ and the propagator $\hat{U}$ into the matrices H and U [5, pp. 6-7].

Thereby, the time development in eq. 2.3 is expressed by

$$\psi_j^{n+1} = e^{-iH\Delta t}\psi_j^n = U(\Delta t)\psi_j^n. \tag{3.4}$$

Expanding the exponential up to the second term leads to

$$\psi_j^{n+1} = (1 - iH\Delta t)\psi_j^n, \tag{3.5}$$

which is equivalent to using the explicit Forward Time Centered Space (FTCS) scheme with $V(x_j) = V_j$

$$\frac{\psi_j^{n+1} - \psi_j^n}{\Delta t} = i\left[\frac{\psi_{j+1}^n - 2\psi_j^n + \psi_{j-1}^n}{(\Delta x)^2} - V_j\psi_j^n\right]. \tag{3.6}$$

This scheme results from the finite difference approximation of the derivative with respect to x and has the advantage of being highly accurate for small time steps. On the other hand, expanding $U^\dagger(\Delta t)$ on the left-hand side gives

$$(1 + iH\Delta t)\psi_j^{n+1} = \psi_j^n, \tag{3.7}$$

which is the same result one obtains by applying the implicit or backward time scheme

$$\frac{\psi_j^{n+1} - \psi_j^n}{\Delta t} = i\left[\frac{\psi_{j+1}^{n+1} - 2\psi_j^{n+1} + \psi_{j-1}^{n+1}}{(\Delta x)^2} - V_j\psi_j^{n+1}\right]. \tag{3.8}$$

Important properties of this scheme are unconditional stability as well as a correct calculation of the equilibrium situation $t \to \infty$. It is, however, important to note that neither of the operators in eq. 3.5 nor in eq. 3.7 is unitary. Therefore, another form needs to be chosen that preserves the hermiticity of the Hamilton operator along with the normalization of the wave function. The proper unitary approximation

$$e^{-iIIt} \simeq \frac{1 - \frac{1}{2}iH\Delta t}{1 + \frac{1}{2}iH\Delta t} \tag{3.9}$$

was introduced by Cayley and further leads to

$$\left(1 + \frac{1}{2}iH\Delta t\right)\psi_j^{n+1} = \left(1 - \frac{1}{2}iH\Delta t\right)\psi_j^n. \tag{3.10}$$

Applying the finite difference approximation results in the Crank-Nicoloson scheme for eq. 2.1, which yields

$$\psi_j^{n+1} - \frac{i\Delta t}{2}\left[\frac{\psi_{j+1}^{n+1} - 2\psi_j^{n+1} + \psi_{j-1}^{n+1}}{(\Delta x)^2} - V_j\psi_j^{n+1}\right] = \psi_j^n + \frac{i\Delta t}{2}\left[\frac{\psi_{j+1}^n - 2\psi_j^n + \psi_{j-1}^n}{(\Delta x)^2} - V_j\psi_j^n\right]. \tag{3.11}$$

This scheme is obtained by forming the average of the explicit and implicit FTCS schemes and combines the accuracy for small time steps with unconditional stability. In order to solve this tridiagonal system of linear equations the $J \times J$ matrices

$$U_1 = \begin{pmatrix} b_1 & a & & & \\ a & b_2 & a & & \\ & \ddots & \ddots & \ddots & \\ & & a & b_{J-1} & a \\ & & & a & b_J \end{pmatrix} \quad \text{and} \quad U_2 = \begin{pmatrix} c_1 & -a & & & \\ -a & c_2 & -a & & \\ & \ddots & \ddots & \ddots & \\ & & -a & c_{J-1} & -a \\ & & & -a & c_J \end{pmatrix} \tag{3.12}$$

are introduced with the coefficients

$$a = -\frac{i\Delta t}{2\Delta x^2}, \quad b_j = 1 + \frac{i\Delta t}{2}\left(\frac{2}{\Delta x^2} + V_j\right), \quad c_j = 1 - \frac{i\Delta t}{2}\left(\frac{2}{\Delta x^2} + V_j\right). \tag{3.13}$$

Thus, eq. 3.11 can be rewritten in the following way [2, pp. 97-98]:

$$U_1 \psi^{\mathbf{n+1}} = U_2 \psi^{\mathbf{n}}. \tag{3.14}$$

The column vector $\psi^{\mathbf{n}}$ contains all spatial wave function values, described by the index j, for every time step n. Eventually, matrix left division is performed in Matlab by using the mldivide command, which can also be executed using \. Since the tridiagonal sparse form does not change, an efficient way to solve eq. 3.14 is by LU-decomposition, where U_1 is split up into a product of a lower and upper triangular matrix. This is combined with forward- and back-substitution for each time step. As all terms in the right-hand side expression are known, it is rewritten as $\mathbf{r^n}$. With this, eq. 3.14 becomes

$$\begin{pmatrix} 1 & 0 & 0 & \dots & 0 \\ m_2 & 1 & 0 & \dots & 0 \\ 0 & m_3 & 1 & \dots & 0 \\ \vdots & \vdots & \vdots & \vdots & \vdots \\ 0 & 0 & 0 & \dots & 1 \end{pmatrix} \underbrace{\begin{pmatrix} u_1 & a & 0 & \dots & 0 \\ 0 & u_2 & a & \dots & 0 \\ \vdots & \vdots & \vdots & \vdots & \vdots \\ \dots & \dots & \dots & \dots & a \\ 0 & 0 & 0 & \dots & u_J \end{pmatrix} \begin{pmatrix} \psi_1^{n+1} \\ \psi_2^{n+1} \\ \vdots \\ \vdots \\ \psi_J^{n+1} \end{pmatrix}}_{\equiv \mathbf{y^{n+1}}} = \begin{pmatrix} r_1^n \\ r_2^n \\ \vdots \\ \vdots \\ r_J^n \end{pmatrix}, \tag{3.15}$$

With $u_1 = b_1$ and $y_1^{n+1} = r_1^n$ the following set of equations is obtained:

$$m_j = a/u_{j-1}, \quad u_j = b_j - m_j a, \quad y_j^{n+1} = r_j^n - m_j y_{j-1}^{n+1}, \quad j = 2, \cdots, J. \tag{3.16}$$

Performing back-substitution yields the solution vector for the n+1 time step [2, p. 47]:

$$\psi_J^{n+1} = y_J^{n+1}/u_J, \quad \psi_j^{n+1} = \left(y_j^{n+1} - a\psi_{j+1}^{n+1}\right)/u_j \quad \text{for} \quad j = J-1, \cdots, 1. \tag{3.17}$$

Due to the high sparsity of the matrices in 3.14, they are created using the spdiags command.

```
psiout = zeros( n, nt ); %matrix of wave function values
psiout( :, 1 ) = psit; %initial wave function

%  Crank-Nicoloson
for it = 2:nt
  psit = ( one + 0.5i * dt * ham ) \ ( ( one - 0.5i * dt * ham ) * psit );
  psiout( :, it ) = psit;
  if mod( it, 5 ) == 0
    set( h, 'YData', scale * abs( psit ) );
    drawnow; %creation of time evolution animation
  end
end
```

Fig. 3.1: Matlab implementation of the Crank Nicoloson scheme.

Fig. 3.1 shows a section of a Matlab function that takes an initial wave function `psit`, spatial grid points `x`, a potential `v` and the matrix `ham`, representing the Hamilton operator, as an input. The output consists of `psiout`, a matrix containing the spatial wave function vectors for every time step and `tout`, the temporal grid vector. The calculation of the input elements can be taken from fig. 3.2.

```
dx = x( 2 ) - x( 1 );
e = ones( n, 1 );
lap = spdiags( [ e, - 2 * e, e ], - 1 : 1, n, n ); %tridiagonal sparse matrix

if bc == "periodic"
    lap( 1, n ) = 1; %periodic boundary conditions
    lap( n, 1 ) = 1;

elseif bc == "fixed"
    lap( 1, n ) = 0; %fixed boundary conditions
    lap( n, 1 ) = 0;
end

t = - lap / ( 2 * mass * dx ^ 2 ); %kinetic energy
ham = t + spdiags( v( : ), 0, n, n ); %Hamilton matrix
```

Fig. 3.2: Calculation of the input elements.

Passing the the number of spatial grid points `nn`, the spatial grid vector `x`, the potential `v`, the type of boundary conditions `bc` and the mass of the particle `mass` to the function, leads to the calculation of the matrix `ham` [3].

Chapter 4

Results

In order to gain knowledge about directionality of quantum mechanical tunnelling, a numerical simulation is performed using Matlab. The problem under consideration consists of a particle, representing a molecule, subject to a periodic asymmetric potential. For the sake of describing the behaviour in the ground and first excited state, the respective eigenstates were computed and positioned in one potential well as the initial wave functions. The time development and thereby the directionality of motion are calculated by implementing the Crank-Nicoloson scheme described in sec. 3.1 with periodic boundary conditions. Moreover, the calculations are executed setting $\hbar = 1$, the potential height to `V0` $= 20$ and the mass of the particle to `mass` $= 5$.

4.1 Eigenvalues and -states of the single triangular potential well

With the use of the Matlab built-in eigenvalue function eigs, the energy level diagram for the single triangular potential well is calculated. The eigs function takes the Hamilton matrix ham from fig. 3.2 with the potential v being the finite, triangular potential well, the desired number of values `k` and the variable `sigma`, which is set to 'smallestabs', as input. With that, the function returns a diagonal matrix containing the eigenvalues on the main diagonal and a matrix with corresponding eigenvectors as columns. Fig. 4.1 below shows the finite, single well with the respective eigenvalues and -functions. Here, a potential height of 20 and a mass of 5 is used. [3]

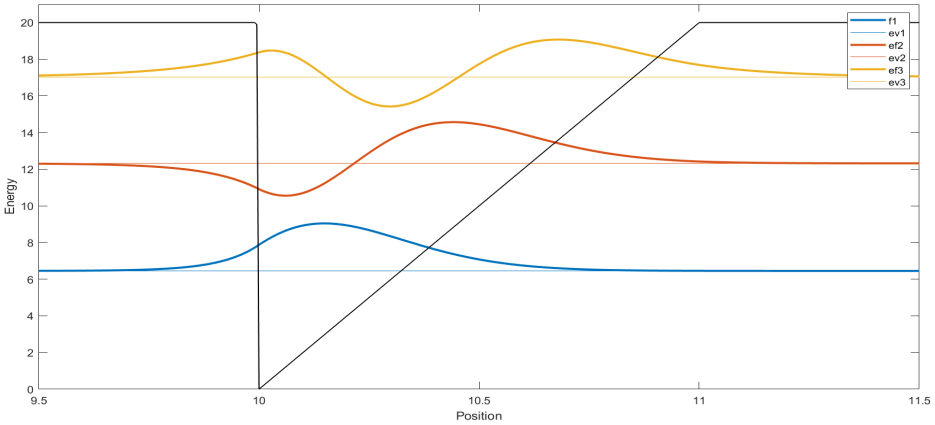

Fig. 4.1: The three lowest energy levels and corresponding wave functions of the finite, single, triangular potential well as a function of position

By comparing fig. 4.1 to fig. 2.2, one can see that the obtained eigenfunctions differ from the airy functions. This is attributable to the finite potential height, which allows a non vanishing contribution and therefore tunnelling also on the left-hand, e.g. steeper slope, side of the well. Hence, these eigenstates will be used as the initial wave functions to study the directionality of tunnelling motion in a periodic, asymmetric potential.

4.2 Directionality of quantum tunnelling

First, the ground state wave function from fig. 4.1 is positioned in the single well around position 10 of a periodic, asymmetric potential with a length of 20. From this initial wave function, the values at later time steps are calculated via the Crank-Nicoloson scheme. Further, the absolute values of the received functions are plotted together with the periodic potential in such a way that the newly computed values replace the previous ones. This yields an animation of the time development of the ground state of a single, triangular potential well inside the periodic, asymmetric case. The starting point of the time evolution as well as the eventual situation after 1000 time steps of 0.005 are shown below in fig. 4.2 and 4.3 respectively. Here, it should be noted that for the sake of better presentation the wave function is normalized and the potential is scaled to a value of 0.5 with the actual potential height being 20.

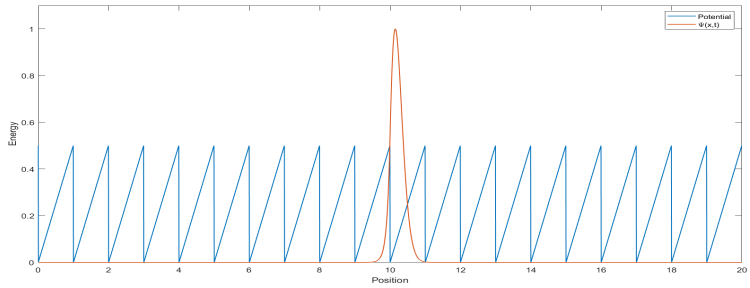

Fig. 4.2: Absolute value of the initial, ground state wave function of the single potential well inside the periodic, asymmetric potential with a height of 20 and a mass of 5. The wave function is normalized and the potential is scaled to a height of 0.5.

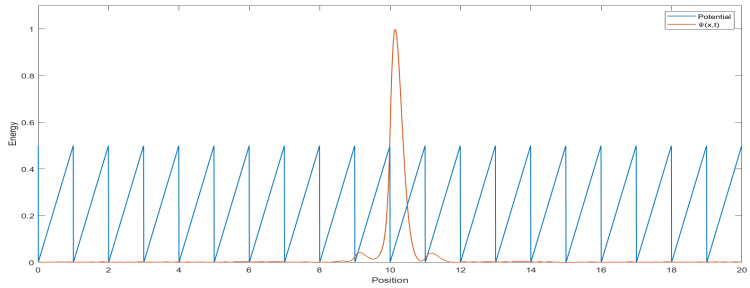

Fig. 4.3: Absolute value of the wave function after 1000 time steps using the ground state of the single potential well as an ansatz inside the periodic, asymmetric potential with a height of 20 and a mass of 5. The wave function is normalized and the potential is scaled to a height of 0.5.

To display the time evolution of the system, the absolute values of the wave function at each of the 1000 time steps are plotted against time using imagesc. This command allows to display the image with scaled colours, representing the probability density of the particle, see fig. 4.4. To emphasize on the directionality of the quantum tunnelling process, the wave function values are split up into parts left and right from the centre of the periodic, asymmetric potential, here position of 10. The first points that are taken into consideration for this calculation, are the ones where the initial wave function values are zero on the right-hand as well as the left-hand side. By adding up the wave function values squared and plotting them against time, one obtains the development of the population inside the potential as an indicator for the directionality, which is shown in fig. 4.5 below.

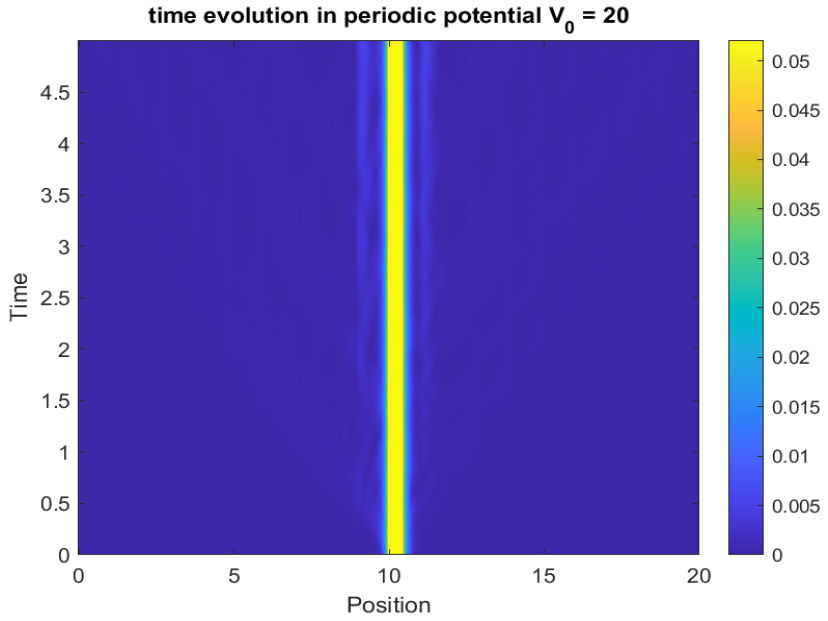

Fig. 4.4: Time evolution of the single well ground state inside the periodic, asymmetric potential. An amplification factor of 2.5 is used for better presentation.

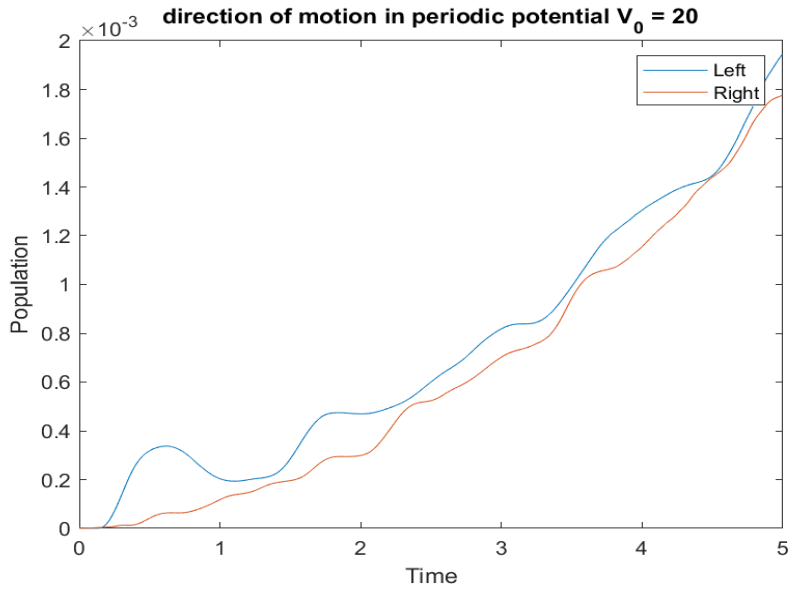

Fig. 4.5: Time evolution of the left- and right-moving population inside the periodic, asymmetric potential for the single well ground state initial wave function.

By looking at fig. 4.2, fig. 4.3 and fig. 4.4, representing the time development of

the system, no preferred direction of the tunnelling motion can be seen. This is underlined by fig. 4.5, as the maximum difference between the evolution of the population to the right- and left-hand side at a certain time point is of order 10^{-4}. Additionally, it can be seen that the tendencies to the directions come close to each other with time. Therefore, no directionality is observed, when the ground state is used as the initial wave function. However, in order to further exemplate the influence of the potential landscape on the motion of the particle, the first excited state is used as the initial wave function. For this situation the same animations and plots as fig. 4.3 - fig. 4.5 with identical settings are created and shown in fig. 4.6 - fig. 4.9 below.

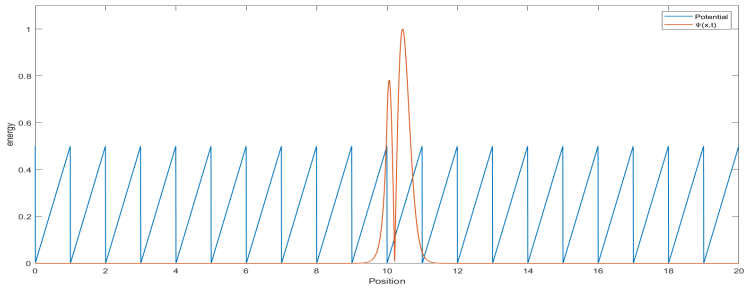

Fig. 4.6: Absolute values of the initial, first excited state wave function of the single potential well inside the periodic, asymmetric potential with a height of 20 and a mass of 5. The wave function is normalized and the potential is scaled to a height of 0.5.

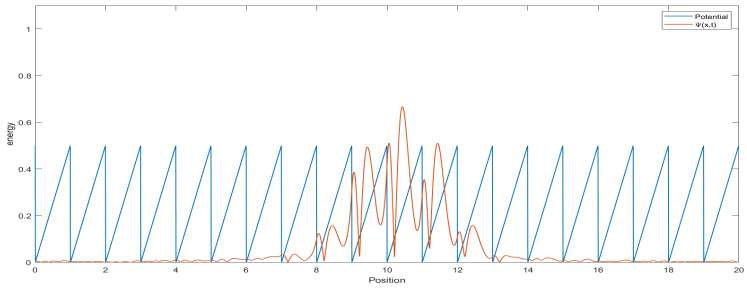

Fig. 4.7: Absolute value of the wave function after 1000 time steps using the first excited state of the single potential well as an ansatz inside the periodic, asymmetric potential with a height of 20 and a mass of 5. The wave function is normalized and the potential is scaled to a height of 0.5.

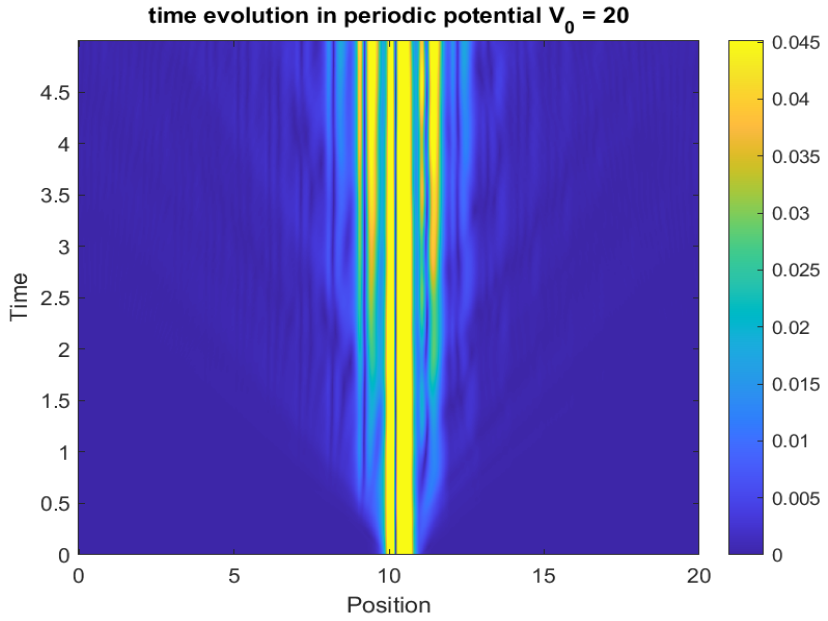

Fig. 4.8: Time evolution of the single well first excited state inside the periodic, asymmetric potential. An amplification factor of 2.5 is used for better presentation.

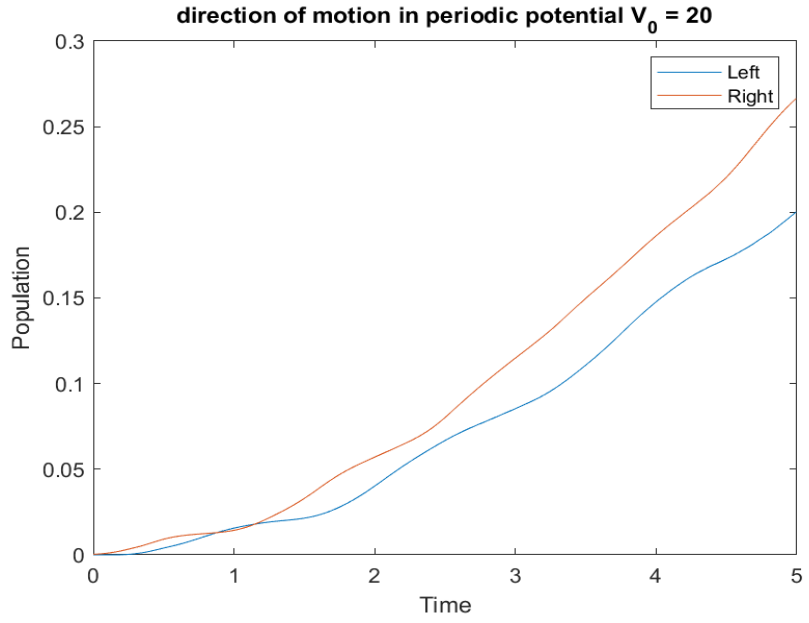

Fig. 4.9: Time evolution of the left- and right-moving population inside the periodic, asymmetric potential for the single well ground state initial wave function.

By comparing the time development of the single well ground state and the first excited state inside the periodic, asymmetric potential, it is evident that in the latter case quantum tunnelling occurs more strongly. In contrast to fig. 4.4 a considerable probability of finding the particle beyond the potential wells directly next to the initial well is apparent in fig. 4.8. Concerning the directionality of motion it can be taken form fig. 4.9 that the first excited state of the single well develops inside the periodic potential preferentially to the right. In the given example, the right-hand side corresponds to the direction of the more gentle slope. Therefore, it can be concluded that the transition from the ground state to the first excited state is connected to a gain of directionality. This behaviour is comparable to the result presented in [1], as it is argued that the dissipating energy leading to directional TR rotation induces the transition from the rotational ground state to a bound state.

4.3 Determination of tunnel rates

In order to quantify the result from sec. 4.2, the tunnel rates for a reduced periodic potential consisting of three potential wells are calculated via eq. 2.7. Here, the basis wave functions are the respective ground and first excited states of the well around position 10 and the directly neighbouring wells to the left and right. These eigenstates are calculated in the same manner as described in sec. 4.1 for different well positions. The hamiltonian $\hat{H}$ in this calculation is identical to the one used in sec. 4.1 with the exception of the potential term for three wells. This leads to the following matrix elements:

$$
\begin{aligned}
&\langle n,k \mid \hat{H} \mid n',k' \rangle \\
&\langle 1,1 \mid \hat{H} \mid 1,1 \rangle = 6.5 \\
&\langle 1,2 \mid \hat{H} \mid 1,1 \rangle = \langle 1,1 \mid \hat{H} \mid 1,2 \rangle = 2.6 \cdot 10^{-4} \\
&\langle 2,1 \mid \hat{H} \mid 1,1 \rangle = \langle 1,1 \mid \hat{H} \mid 2,1 \rangle = 4.8 \cdot 10^{-3} \\
&\langle 2,2 \mid \hat{H} \mid 1,1 \rangle = \langle 1,1 \mid \hat{H} \mid 2,2 \rangle = -2.2 \cdot 10^{-2} \\
&\langle 3,1 \mid \hat{H} \mid 1,1 \rangle = \langle 1,1 \mid \hat{H} \mid 3,1 \rangle = -7.2 \cdot 10^{-8} \\
&\langle 3,2 \mid \hat{H} \mid 1,1 \rangle = \langle 1,1 \mid \hat{H} \mid 3,2 \rangle = 2.5 \cdot 10^{-6} \\
&\langle 1,2 \mid \hat{H} \mid 1,2 \rangle = \langle 3,2 \mid \hat{H} \mid 3,2 \rangle = 12.3 \\
&\langle 2,1 \mid \hat{H} \mid 1,2 \rangle = \langle 1,2 \mid \hat{H} \mid 2,1 \rangle = -1.3 \cdot 10^{-1} \\
&\langle 2,2 \mid \hat{H} \mid 1,2 \rangle = \langle 1,2 \mid \hat{H} \mid 2,2 \rangle = 3.0 \cdot 10^{-1} \\
&\langle 3,1 \mid \hat{H} \mid 1,2 \rangle = \langle 1,2 \mid \hat{H} \mid 3,1 \rangle = -1.5 \cdot 10^{-5} \\
&\langle 3,2 \mid \hat{H} \mid 1,2 \rangle = \langle 1,2 \mid \hat{H} \mid 3,2 \rangle = -7.2 \cdot 10^{-5} \\
&\langle 2,1 \mid \hat{H} \mid 2,1 \rangle = \langle 3,1 \mid \hat{H} \mid 3,1 \rangle = 6.4 \\
&\langle 2,2 \mid \hat{H} \mid 2,1 \rangle = \langle 2,1 \mid \hat{H} \mid 2,2 \rangle = 4.7 \cdot 10^{-2} \\
&\langle 3,1 \mid \hat{H} \mid 2,1 \rangle = \langle 2,1 \mid \hat{H} \mid 3,1 \rangle = 4.8 \cdot 10^{-3} \\
&\langle 3,2 \mid \hat{H} \mid 2,1 \rangle = \langle 2,1 \mid \hat{H} \mid 3,2 \rangle = 2.2 \cdot 10^{-2} \\
&\langle 2,2 \mid \hat{H} \mid 2,2 \rangle = 12.2 \\
&\langle 3,1 \mid \hat{H} \mid 2,2 \rangle = \langle 2,2 \mid \hat{H} \mid 3,1 \rangle = 1.3 \cdot 10^{-1} \\
&\langle 3,2 \mid \hat{H} \mid 2,2 \rangle = \langle 2,2 \mid \hat{H} \mid 3,2 \rangle = 3.0 \cdot 10^{-1} \\
&\langle 3,2 \mid \hat{H} \mid 3,1 \rangle = \langle 3,1 \mid \hat{H} \mid 3,2 \rangle = -4.8 \cdot 10^{-2}
\end{aligned}
\tag{4.1}
$$

Regarding the notation, n and n' denote the wells, with 1 representing the left, 2 the central and 3 the right one. k and k' denote the energy levels, where 1 stands for the ground and 2 for the first excited state. The diagonal elements of the above matrix are the eigenvalues corresponding to the ground and first excited state of the single, triangular well. Further, the non-diagonal elements result from the coupling between the states due to quantum mechanical tunnelling. As the hamiltonian is hermitian, the resulting matrix is symmetric. This is explained by the reduction of the system to three wells. The part of the wave function that propagates through the barrier tunnels back in the other direction. This indicates that carting off the wave function would lead to symmetry breaking and therefore directed motion. Other possibilities would be an expansion of the system to more wells and energy levels as well as a localization of the wave function by environment couplings that results in relaxation. This increase in complexity and computing effort will not be elaborated on in this work. Nevertheless, these possibilities bear potential for finding an underlying explanation concerning the directed quantum tunnelling motion observed in 4.2.

Chapter 5

Conclusion

To conclude, directed quantum tunnelling is apparent when the first excited state of a single triangular well is used as the initial wave function for the time development inside a periodic, asymmetric potential. Yet, no clear directionality is present with the ground state. Therefore, it can be argued that the transition from the ground to the first excited state is correlated to directed tunnelling motion.

The quantification of the obtained result via the calculation of the tunnel rate matrix did not show a breaking of symmetry. This indicates that, in order to investigate on the origin of directed quantum tunnelling and energy dissipation occurring in the process, the example considered needs to be extended from a two-level system to a system that includes additional wells and eigenstates. Moreover, another possibility would be the localization of the wave function by environment couplings.

Bibliography

[1] S. Stolz, O. Groening, J. Prinz, H. Brune, R. Widmer. *Molecular motor crossing the frontier of classical to quantum tunneling motion.* Proceedings of the National Academy of Sciences **117** (2020) 14838 .

[2] P. Puschnig. Computerorientierte Physik, 2016. https://physik.uni-graz.at/~pep/CompOriPhys/CoP.pdf

[3] MATLAB. *9.7.0.1190202 (R2019b).* The MathWorks Inc., Natick, Massachusetts, 2019.

[4] H. G. Evertz, W. von der Linden. Quantenmechanik, 2019. https://itp.tugraz.at/LV/evertz/QM_Skript/qm_2019.pdf

[5] L. Viklund, L. Augustsson, J. Melander. Numerical approaches to solving the time-dependent Schrödinger equation with different potentials, 2016. http://uu.diva-portal.org/smash/get/diva2:935561/FULLTEXT01.pdf

[6] G. Binnig, H. Rohrer. *Scanning tunneling microscopy.* IBM Journal of Research and Development **44** (2000) 279. doi:10.1147/rd.441.0279

[7] L. Esaki, Y. Miyahara. *A new device using the tunneling process in narrow p-n junctions.* Solid-State Electronics **1** (1960) 13. doi:https://doi.org/10.1016/0038-1101(60)90052-6

[8] G. Meliolla, A. Surawijaya, M. A. Sulthoni, T. Adiono. Study of tunneling gate oxide and floating gate thickness variation effects to the performance of split gate flash memory. *2017 International Symposium on Electronics and Smart Devices (ISESD)*, 2017 S. 256–259. doi:10.1109/ISESD.2017.8253343

[9] F. Trixler. *Quantum Tunnelling to the Origin and Evolution of Life.* Current organic chemistry **17** (2013) 1758. doi:10.2174/13852728113179990083

[10] V. Jain. A discussion of particles in triangular potentialwells and the quantum harmonic oscillator, 2019.
https://mazziotti.uchicago.edu/journal/jain_v.pdf

[11] S. Birner. nextnano3 - Tutorial Triangular well. Last accessed 04 April 2021.
https://www.nextnano.com/nextnano3/tutorial/1Dtutorial_GaAs_triangular_well.htm

[12] M. Barcenas, Y. Reyes-Mercado, A. Romero-Martínez, G. Odriozola, P. Orea. *Coexistence and interfacial properties of a triangle-well mimicking the Lennard-Jones fluid and a comparison with noble gases.* The Journal of chemical physics **142** (2015) 074706.
doi:10.1063/1.4909548

[13] S. Yukawa, G. Tatara, M. Kikuchi, H. Matsukawa. *Quantum ratchet.* Physica B: Condensed Matter **284-288** (2000) 1896.
doi:https://doi.org/10.1016/S0921-4526(99)02982-8

[14] S. Ethier, J. Lee. *The flashing Brownian ratchet and Parrondo's paradox.* Royal Society Open Science **5** (2017).
doi:10.1098/rsos.171685